JOURNAL OF THERMOPHYSICS AND HEAT TRANSFER
Vol. 24, No. 1, January–March 2010

Nonlinear Heat Conduction in Isotropic and Orthotropic Materials with Laser Heat Source

E. Fong,* T. T. Lam,† and S. E. Davis‡
The Aerospace Corporation, El Segundo, California 90245-4691

DOI: 10.2514/1.42806

Although the convective cooling of simple materials undergoing laser irradiation has been well documented, the effects of radiative cooling for composite materials undergoing laser heating are not as well documented and are of increasing importance to the manufacturing and aerospace industries. The temperature distributions within one-dimensional homogeneous and two-dimensional orthotropic radiating plates subjected to a spatially decaying laser source are presented. The incident energy at the exposed external surface is partially absorbed and transferred through the plate by conduction. The temperature results are presented as a function of a wide variety of thermal and geometric dimensionless parameters. The effects of surface radiation and material conductivity are examined in detail. Results from this study are compared to data in the open literature to gain a better understanding of the effects that the fourth power law for radiation, local temperature gradient in conduction, and first power of the temperature difference in convection have on the resultant temperature profiles.

Nomenclature

A_i	=	area of node i
Bi	=	Biot number, $h/\mu k$
C_i	=	nodal capacitance, J/K
C_p	=	specific heat, J/kg · K
d	=	laser beam diameter, m
F_{ij}	=	view factor between nodes i and j
G_{ij}	=	linear or radiation conductance, W/K
$\dot{g}$	=	Gaussian spatial profile of the laser
$\dot{g}'''$	=	energy generation rate per unit volume, W/m^3
h	=	convective heat transfer coefficient, W/m^2 · K
I_o	=	laser peak power density, W/m^2
k	=	thermal conductivity, W/m · K
L	=	thickness of the plate, m
n	=	total number of nodes of the thermal math model
Q_i	=	heat source, W
R	=	surface reflectance
T	=	present temperature, K
T_c	=	external environment temperature for convective exchange, K
T_o	=	initial temperature, K
T_r	=	external environment temperature for radiative exchange, K
T'	=	unknown temperature, K
T''	=	past temperature, K
T^*	=	dimensionless temperature, $(T - T_o)/[I_o(1 - R)/\mu k]$
t	=	time, s
W	=	half-width of the plate, m
x	=	x coordinate, m
y	=	y coordinate, m
y^*	=	depth, $\mu\, y$
α	=	thermal diffusivity, m^2/s
δ	=	laser-pulse fall-time parameter, 1/s
ε	=	emissivity
θ	=	laser-pulse rise-time parameter, 1/s
μ	=	absorption coefficient, 1/m
ρ	=	density, kg/m^3
σ	=	Stefan–Boltzmann constant, 5.67×10^{-8} W/m^2 · K^4
τ	=	dimensionless time, $t\alpha\mu^2$

Subscripts

e	=	external
i	=	current node
j	=	adjacent node
o	=	initial
x	=	x direction
y	=	y direction
1	=	surface 1
2	=	surface 2

Presented as Paper 3807 at the 40th Thermophysics Conference, Seattle, WA, 23–26 June 2008; received 17 December 2008; revision received 29 July 2009; accepted for publication 27 September 2009.

*Member of the Technical Staff, Spacecraft Thermal Department. Member AIAA.
†Director, Spacecraft Thermal Department. Associate Fellow AIAA.
‡Senior Member of the Technical Staff, Spacecraft Thermal Department. Member AIAA.

I. Introduction

COMPOSITES have become an integral structural material for various space and terrestrial engineering applications in recent years due to their lightweight construction and high heat strength. However, characterizing the thermal response within such a material is difficult due to the mathematical complexity of the governing equations. Intense heating produced by laser irradiation can adversely affect the integrity of composite structures due to the rapid degradation of mechanical properties [1]. Damage to materials caused by high-energy laser exposure is a strong function of material thermal response. Therefore, the accurate modeling of the thermal response constitutes an important element in assessing the overall reliability of composite structures subjected to high-power laser heating.

Various investigations on the study of laser heating have been conducted in the past. Most of these studies are limited to a configuration of semi-infinite medium with a variety of heating profiles. Ready [2] studied the effects of high-power laser incidence on absorbing opaque surfaces. Dabby and Paek [3] analytically investigated the material removal process from the front surface of a solid heated by a high-intensity laser. Blackwell [1] modeled the effect of continuous laser heating of a semi-infinite slab with convection on the surface of incidence. These studies revealed that for certain laser and material parameters, interior temperatures of the solid could exceed the surface temperature, which could result in catastrophic failure without melting or burning through the surface. In recent years, Chaudhry and Zubair [4], Zubair and Chaudhry [5,6], and

Yilbas [7] investigated one-dimensional conduction in a semi-infinite solid for various types of laser profiles by using the classical Laplace transform technique. All of the aforementioned studies were limited to semi-infinite solids and constant or decaying lasers.

Cheung et al. [8] studied the heating effect on finite slabs subjected to laser-pulse irradiation and convective cooling. Peterson et al. [9] investigated the temperature distribution within a two-dimensional rectangular slab subjected to a time-varying and spatially decaying laser source. Closed-form analytical solutions were obtained in these two studies with the application of the integral-transform technique. The two-dimensional model improved upon prior one-dimensional models as well as models limited to semi-infinite media.

It has been shown in these previous studies that high-powered laser heating coupled with strong convection at the exposed surface can lead to bursting of the material when sufficient incident energy is absorbed within the solid. This phenomenon could be attributed to the cooling of the exposed surface while a localized temperature maximum exists within the material. In the case of no convection, radiation cooling can also lead to the same problem if the material has certain characteristics such as low thermal conductivity and high surface-IR emissivity. Therefore, vacuum conditions encountered in manufacturing or space applications in which a material is heated by a laser (or any point source heating at the surface) can experience this bursting phenomenon.

Most of the aforementioned investigations are for convective cooling only. However, most realistic problems encountered in high-temperature engineering applications involve radiative cooling. When radiation exchange with the environment is considered, the heat conduction equation will be coupled to nonlinear boundary conditions that correlate to surface temperature to the fourth power. As a result, a numerical solution is sought to obtain the temperature profile within the solid. The purpose of this study is to develop a thermal model to investigate the heat conduction phenomenon in metallic and composite materials subjected to high-energy laser irradiation. The thermal response within the material will be studied in detail with particular emphasis on the absorbed intensity of the laser source, material properties, and surface cooling effects. This study will present a new solution for the simulation of laser heating of metals and composites. These results will provide further insight into the behavior of laser-irradiated materials under high-temperature conditions, which may be used to increase the reliability of thermal systems.

In Sec. II, we provide formulations that govern heat conduction associated with internal energy generation in isotropic and orthotropic materials. Moreover, the laser profiles for these two configurations are discussed in detail in this section. Since the governing partial differential equation is posed as a nonlinear problem, a numerical solution will be obtained by using the Systems Improved Numerical Differencing Analyzer (SINDA) software [10]. Details of the thermal model are briefly described in the Appendix. Section III provides the results and discussion for both an isotropic and orthotropic case. The purpose of the isotropic case is to validate the current numerical model as well as to investigate the primary parameters affecting a material's thermal response. The orthotropic case is presented to examine two-dimensional composite effects. A summary of the study and plans for future work are discussed in Sec. IV.

II. Heat Conduction with Internal Energy Generation

A. Isotropic Material and Uniform Laser Irradiation

A schematic of an isotropic plate is shown in Fig. 1. It is assumed that the plate has uniform thickness and its radiative properties are diffuse gray. A portion of the laser energy incident on the upper boundary is reflected and radiated away from the surface to the environment at T_r. The transmitted portion of the laser energy is attenuated as it propagates through and becomes absorbed within the material. The remaining energy will be transmitted through the bottom surface and radiated to the external environment at T_r [11,12]. Energy may also be carried away through convection if the plate is not in vacuum.

The energy equation governing conduction in an isotropic plate is given by

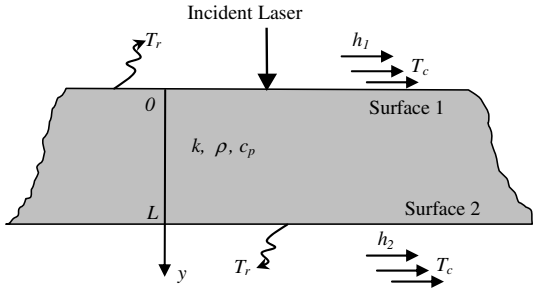

Fig. 1 Schematic of a finite plate subjected to spatially and temporally decaying laser heating.

$$k_y \frac{\partial^2 T}{\partial y^2} + \dot{g}''' = \rho C_p \frac{\partial T}{\partial t} \quad \text{in } 0 < y < L \tag{1}$$

where $\dot{g}'''$ denotes the energy generation rate per unit volume inside a material subjected to internal laser energy absorption. The energy source term for laser application can be written as [2]

$$\dot{g}'''(y,t) = I_o \mu (1-R) e^{-\mu y} (e^{-\theta t} - e^{-\delta t}) \tag{2}$$

where I_o is the laser peak power density, θ and δ are laser-pulse parameters, R is the surface reflectivity of the solid dependent on the wavelength of the incident laser, and μ is the absorption coefficient.

The exponential function in Eq. (2) accounts for the attenuation, rise, and fall times of the laser pulse. The laser beam parameters chosen for this analysis are as follows: the wavelength is 1000 nm, maximum pulse peak power density $I_o = 24$ GW/cm^2, pulse length is 25 ns, $\theta = 4.9 \times 10^7$ 1/s, and $\delta = 2.45 \times 10^8$ 1/s. The parameters were approximately based on the characteristics of a Lambda Physik Powergator PG1064-30 laser and used a pulse parameter ratio $\theta/\delta = 1/5$ [7]. The laser energy $\dot{g}'''$ incident at the surface $y = 0$ is illustrated in Fig. 2 of [9].

The boundary conditions at the upper and lower surfaces are

$$k_y \frac{\partial T}{\partial y} = \varepsilon_1 \sigma (T^4 - T_r^4) + h_1 (T - T_c) \quad \text{at } y = 0, \qquad t > 0 \tag{3a}$$

$$-k_y \frac{\partial T}{\partial y} = \varepsilon_2 \sigma (T^4 - T_r^4) + h_2 (T - T_c) \quad \text{at } y = L, \qquad t > 0 \tag{3b}$$

For Eq. (3), it is assumed that the external environment radiative and convective sink temperatures are T_r and T_c, respectively. Furthermore, it is assumed that heat losses from the end edges of the plate are small, so insulated edge boundary conditions are used. The initial condition in the region is

$$T = T_o \quad \text{for } t = 0 \tag{4}$$

B. Orthotropic Material and Spatially Decaying Laser

A schematic of an orthotropic radiating plate is shown in Fig. 2. The configuration is similar to the isotropic formulation described above, except that the incident laser is spatially varying in the x direction and that no convection is present.

The energy equation governing the conducting orthotropic plate is given by

$$k_x \frac{\partial^2 T}{\partial x^2} + k_y \frac{\partial^2 T}{\partial y^2} + \dot{g}''' = \rho C_p \frac{\partial T}{\partial t} \quad \text{in } 0 < x < W, \qquad 0 < y < L \tag{5}$$

where $\dot{g}'''$ denotes the energy generation rate per unit volume inside a material. The energy source term for laser application can be written as [2]

$$\dot{g}'''(x,y,t) = I_o \mu (1-R) e^{-8x^2/d^2} e^{-\mu y} (e^{-\theta t} - e^{-\delta t}) \tag{6a}$$

Equation (6a) specifies the variation in laser intensity with respect to space and time. The parameters I_o, θ, δ, R, and μ are defined

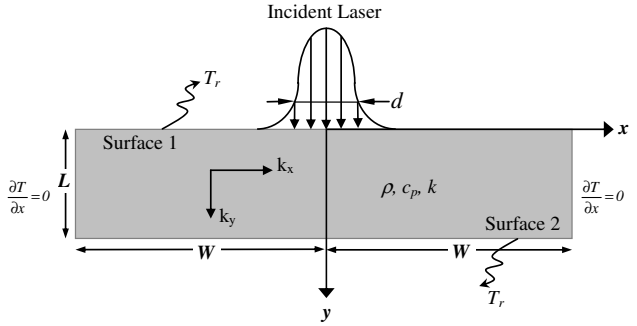

Fig. 2 Schematic diagram of an orthotropic radiating plate subjected to spatially decaying laser heating.

previously for the isotropic case. The beam diameter d is 5 mm. It is suitable to model the laser intensity as having a Gaussian distribution,

$$\dot{g}(x, y = 0, t = 0) = \exp(-8x^2/d^2) \tag{6b}$$

as depicted in Fig. 3 of [9], which is typical of many lasers [2]. With respect to the variation in laser intensity in the through-thickness direction as well as the spreading in the horizontal direction, Eq. (6a) captures the attenuation of the laser beam by the material.

The boundary conditions at the upper and lower surfaces are

$$k_y \frac{\partial T}{\partial y} = \varepsilon_1 \sigma (T^4 - T_r^4) \quad \text{at } y = 0 \quad \text{for all } x, \qquad t > 0 \tag{7a}$$

$$-k_y \frac{\partial T}{\partial y} = \varepsilon_2 \sigma (T^4 - T_r^4) \quad \text{at } y = L \quad \text{for all } x, \qquad t > 0 \tag{7b}$$

Similar to the boundary conditions in the isotropic material case, Eq. (7) assumes that energy is dissipated into an external environment sink temperature T_r. Again, it is assumed that heat losses from the end edges of the plate are small, so insulated edge boundary conditions are used. Because of symmetry, one can perform the analysis based on the half-width of the slab under consideration. The boundary conditions are given by

$$\frac{\partial T}{\partial x} = 0 \quad \text{at } x = 0 \quad \text{for all } y, \qquad t > 0 \tag{7c}$$

$$\frac{\partial T}{\partial x} = 0 \quad \text{at } x = W \quad \text{for all } y, \qquad t > 0 \tag{7d}$$

The initial condition in the region is

$$T = T_o \quad \text{for } t = 0 \tag{8}$$

For plates having a finite thickness, an integral-transform technique has been used successfully to obtain analytical solutions for the temperature distribution within the plates, provided that the boundary conditions are linear [8,9]. A general solution has been developed by Özisik [13] using this technique. However, because radiation has a fourth-order dependence on temperature, an analytical solution cannot easily be obtained. To understand the effects of radiation on a finite plate, a thermal model was built and solved via a finite difference method. More details on the solution subroutines used to construct the thermal model and predict the temperatures are described in the Appendix.

III. Results and Discussion

The analysis is performed by building and executing a SINDA thermal math model. The model consists of 35 unevenly spaced nodes in the through-thickness direction, with more nodes near the surface to capture thermal gradients and three nodes by three nodes evenly spaced in the planar directions. The plate area on the top and bottom surfaces are fixed at 30 by 30 mm, with the plate thickness L varied as a parameter. The laser energy is modeled as a heat source that illuminates the center nodes of the plate. It was found during the analysis that under the short time scales involved in this problem, not much heat travels outward in the planar direction. Therefore, it is appropriate to make the assumption that the sides of the plate are adiabatic. Material properties are defined and varied during the course of the parametric study. Finally, the external environment T_r and T_c and initial temperatures T_o are set to 0°C.

A. Isotropic Material and Uniform Laser Irradiation

1. *Verification of the Thermal Math Model*

The physical problem under consideration has been solved analytically by Cheung et al. [8] for a finite slab subjected to convective cooling at the lower and upper boundaries with an environment at zero temperature ($T_c = 0$°C) and the slab initially at a uniform temperature of 0°C ($T_o = 0$°C). In their paper, the thermal response of the material was illustrated via temperature profiles for a given set of Biot numbers and times. It was found that the maximum temperature of the material is located beneath the surface and that the depth of this location is a strong function of both Biot number and time. In [8], the Biot number, which is used to compare surface to interior heat transfer effects, was defined as $h/\mu k$, where h is the heat transfer coefficient at the surface, μ is the absorption coefficient of the slab, and k is its thermal conductivity. The absorption coefficient μ was used in place of the typical characteristic length, because laser applications use μ to determine the penetration depth of the laser into a material.

To validate the model for the present study, test cases were generated for comparison with the analytical results generated by Cheung et al. [8]. The thermophysical and optical properties for the material used for the simulations are as follows: $k = 156$ W/m · K, $\rho = 2330$ kg/m^3, $C_p = 713$ J/kg · K, $\mu = 4952.65$ 1/m, and $R = 0.3186$ [14,15]. Figure 3a shows the through-thickness temperature profile for the case of a 0.1-mm-thick plate subjected to convective cooling. The convective heat transfer coefficient applied to the upper (laser-irradiated) surface is 3.86×10^6 W/m^2 · K, which is equivalent to a Biot number ($h_1/\mu k$) of 5.0. The lower surface is subjected to a much smaller convective heat transfer coefficient of 50 W/m^2 · K. A large heat transfer coefficient was used on the irradiated surface to clearly demonstrate the effect that convective cooling has on the peak-temperature location of the plate. Figure 3b shows temperature profiles for the case of a 1.0-mm-thick plate. Both figures show data generated by the numerical model and the analytical solution [8]. Further discussion about the spatial and temporal responses for various Biot number conditions can also be found in Cheung et al. [8].

Results reveal that the present numerical model compares very well with the analytical model; the maximum difference is less than 1% between these two models. Note that the peak temperature is located inside the slab rather than at the surface, because the convective cooling lowers the temperature at the irradiated surface faster than the laser can heat the same area. Convective cooling becomes more pronounced with increasing Biot number and time. The temperature peaks are more noticeable for larger Biot numbers, because a larger Biot number leads to higher convective heat transfer at the surface, assuming constant conductivity and geometry. These features are clearly demonstrated by both the analytical and the numerical models.

2. *Comparison of Convective and Radiative Boundary Cooling*

As previously noted, the physical problem under consideration has been solved analytically for one-dimensional [8] and two-dimensional [9] finite slabs subjected to convective cooling at the lower and upper surfaces with an environment at zero temperature ($T_c = 0$°C) and the slab initially at a uniform temperature ($T_o =$ 0°C). However, most realistic problems encountered in high-temperature engineering applications involve radiative cooling at the boundaries, leading to nonlinear boundary conditions. There is no general closed-form solution available for such nonlinear partial differential equations. Thus, the model developed with the SINDA

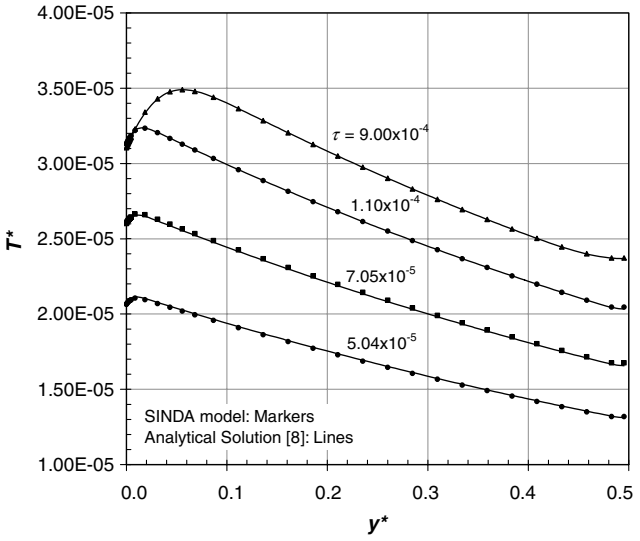

a)

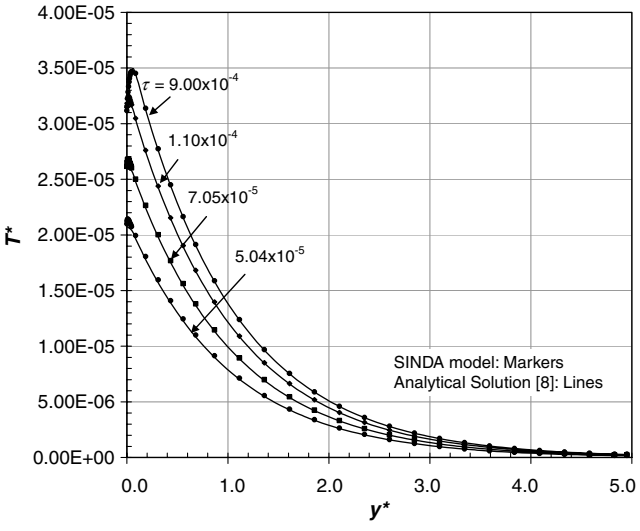

b)

Fig. 3 Temperature profile comparison between SINDA model data and an analytical solution with convection boundary condition for a) 0.1 mm plate and b) 1 mm plate.

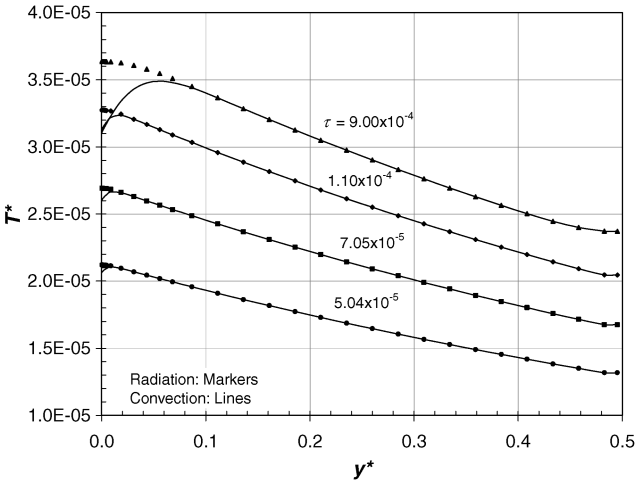

a)

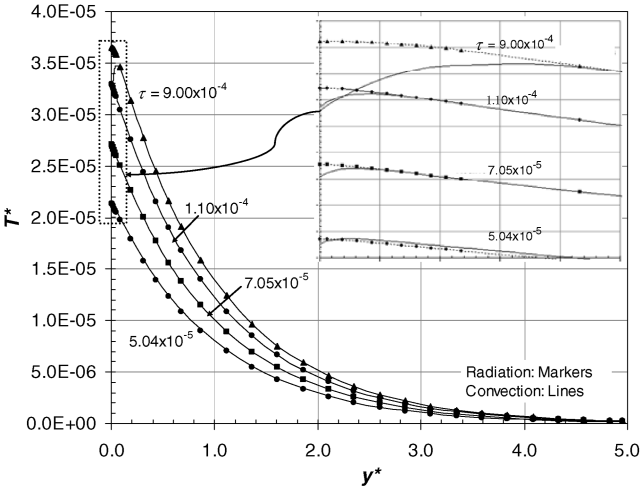

b)

Fig. 4 Temperature profile of radiation boundary condition at various times for a) 0.1 mm plate and b) 1 mm plate.

analyzer is a useful tool for analyzing nonlinear heat conduction problems.

The results presented in Fig. 4 compare through-thickness thermal profiles for convective and radiative boundary conditions at various times using the same laser pulse. For the convective boundary condition, the peak temperature is located inside the material rather than at the surface (as noted previously). However, for the radiative case, the maximum temperature is located much closer to the irradiated surface. The difference in the location of maximum temperature rise is due to the vast difference in heat transfer coefficients. A Biot number equal to 5.0, as seen in the convective case, corresponds to a heat transfer coefficient of 3.86×10^6 W/m$^2 \cdot$ K. To achieve an equivalent Biot number for radiation, either the effective thermal conductivity must be greatly reduced or the surface temperature must be increased to enhance radiative cooling.

3. *Effect of Variation in Thermal Conductivity on Temperature Profile*

Material properties such as thermal conductivity and absorption coefficient can be varied to gain a better understanding of their effect on thermal response. For the purpose of this analysis, the thermal conductivity will be investigated while keeping other parameters such as emissivity and thermal capacitance ρC_p fixed. Note that the thermal diffusivity α will change as a result of varying conductivity, which in turn influences the time constant τ.

Three values of thermal conductivity have been selected to demonstrate its effect on the thermal response of a material. The values chosen cover a wide range of materials, from low-conductivity composites such as carbon fiber to high-conductivity metals such as aluminum. Figure 5 shows the through-thickness temperature

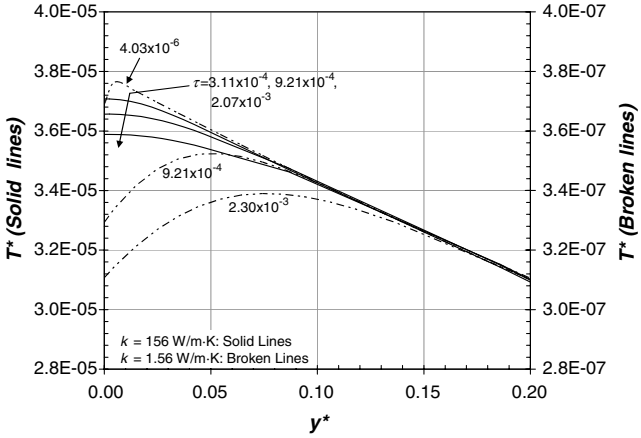

Fig. 5 Effect of thermal conductivity on temperature profiles at various times.

distribution as a function of depth on a 1-mm-thick plate for thermal conductivity values of 156 W/m · K (solid lines) and 1.56 W/m · K (broken lines). The time constants used in the figure are meant to illustrate the time at which the material reaches its maximum temperature and, subsequently, the extent of the temperature decay at specified times. Note that as thermal conductivity decreases, the shape of the temperature peaks becomes more pronounced. Also note that the difference in the orders of magnitude between the temperature scales is the consequence of its nondimensionalization as a function of k, and as such, the magnitudes of the unscaled temperature profiles relative to each other may be read directly from the plot. Thus, the lower-conductivity model can be seen to yield a higher peak-temperature response than the higher-conductivity model, as one would expect, assuming that both are heated identically. Finally, it may be seen in Fig. 5 that the maximum temperature reached by the lower-conductivity material is located beneath the surface, similar to the convection case.

Figure 6 shows plots of temporal temperature profiles at specific locations for three different values of thermal conductivity. For a higher-conductivity material, as shown in Fig. 6a, the surface and the interior temperature response are of similar magnitude. However, as conductivity decreases, it becomes more apparent that the temperature in the interior of the plate is higher than the surface temperature, similar to the effects of the convection case presented earlier (bear in mind that the difference in the exponent of the T^* scale is solely due to scaling by the conductivity). Additionally, the peak-temperature rise occurs faster for materials with a lower thermal conductivity. This effect is due to the slower dissipation of heat through the material and can be seen clearly by comparing the three plots in Fig. 6.

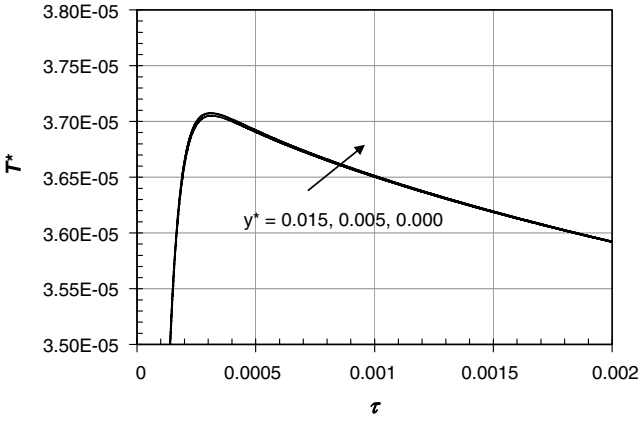

a)

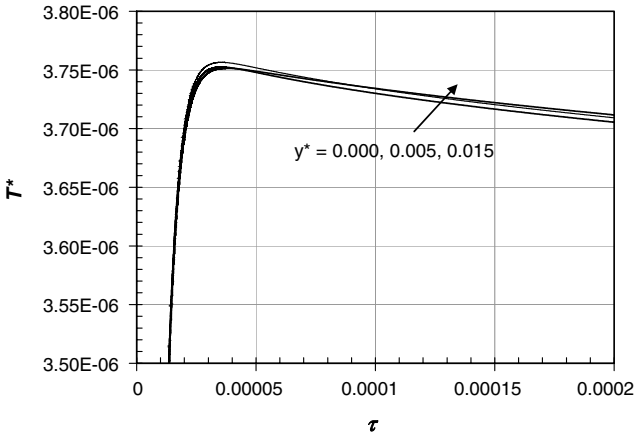

b)

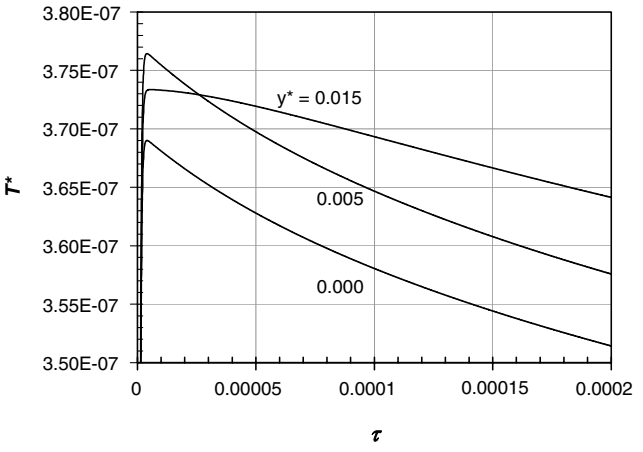

c)

Fig. 6 Effect of thermal conductivity on temporal temperature response at various locations for 1 mm plate: a) $k = 156$ W/m · K, b) $k = 15.6$ W/m · K, and c) $k = 1.56$ W/m · K.

4. *Comparison of Pure Convective and Convective Plus Radiative Boundaries Cooling*

As a further illustration of the nonlinear effect of radiation at the boundary, Fig. 7 depicts the effective heat transfer coefficients for the case of pure convection and the case with combined convection and radiation at the boundary. Temperature differences between these two cases are shown for different Biot numbers. The convective cooling effects are dominant with a Biot number equal to 500, where the same heat transfer coefficient of 3.86×10^6 W/m^2 · K was used, but the material conductivity was reduced to $k = 1.56$ W/m · K (compared to the 156 W/m · K value used in Fig. 4). For this particular case, results clearly demonstrate that convective heat transfer is a dominant factor in surface cooling, since there are no significant differences in terms of surface temperatures ($\Delta T \approx 0$) when comparing the case with pure convection to combined convection and radiation. However, as the Biot number is decreased, which implies that the convective cooling effect at the surface is weakening, radiative cooling will become a principal factor in cooling of solids. One can see from Fig. 7 that as the Biot number is decreased from 500 to 0.5, the temperature difference increases from a negligible amount to over 120 K. The results show that the radiative cooling effect becomes a more significant factor as compared to convection for a small Biot number. In other words, the effect of radiative cooling is an influential factor in certain high-temperature applications in the manufacturing and aerospace industries when convection is a secondary factor.

B. Orthotropic Material and Spatially Decaying Laser

Consider heating a composite material with the following thermophysical properties (typical for a carbon fiber composite):

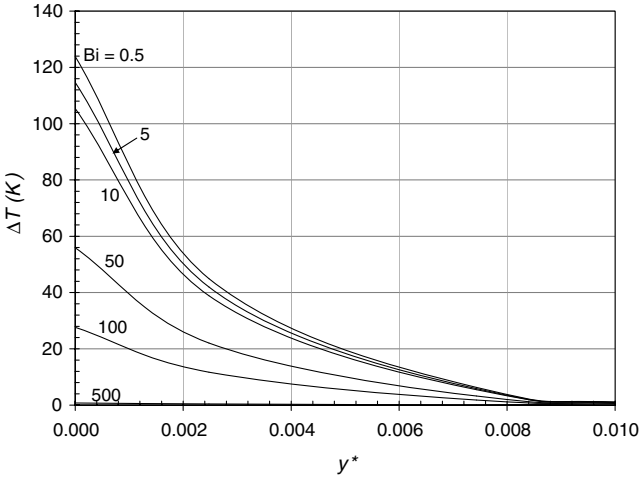

Fig. 7 Comparison between pure convective vs convective plus radiative boundary conditions for a 1 mm plate.

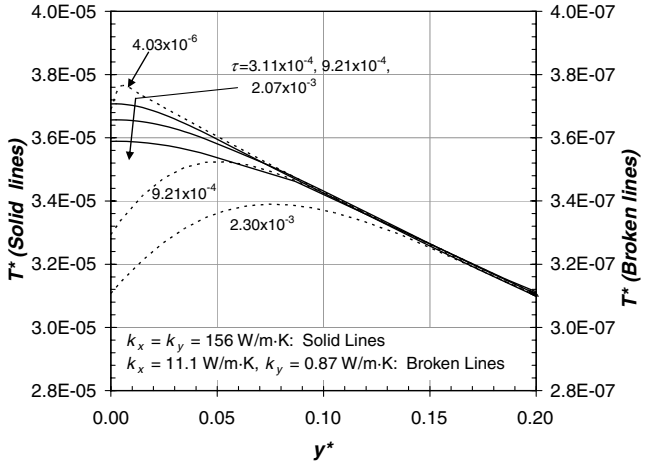

Fig. 8 Thermal conductivity effect on the temperature profiles.

$k_x = 11.1$ W/m · K, $k_y = 0.87$ W/m · K, $\rho = 1400$ kg/m^3, and $C_p = 935$ J/kg · K [16]. The material will be subjected to a spatially decaying laser, as shown in Fig. 2, with a Gaussian profile given by Eq. (6a).

1. Effect of Thermal Conductivity

Figure 8 shows the centerline temperature profile near the irradiated surface at various times for two different materials. The solid line corresponds to the isotropic material properties used earlier,

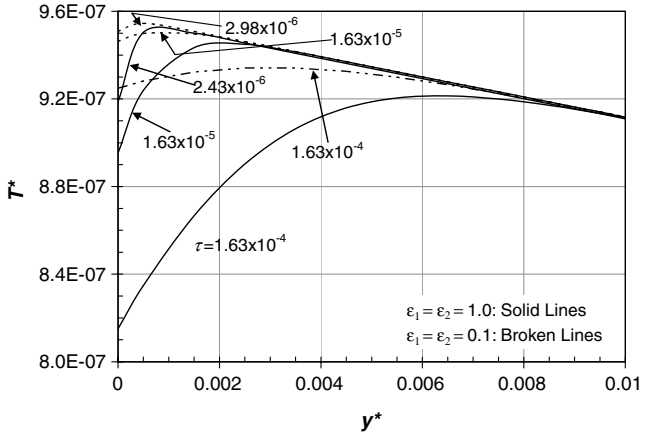

Fig. 9 Centerline temperature profiles in a 1-mm-thick composite ($k_x = 11.1$ W/m · K and $k_y = 0.87$ W/m · K) for two different emissivities using a high-power laser ($I_o = 24$ GW/cm^2).

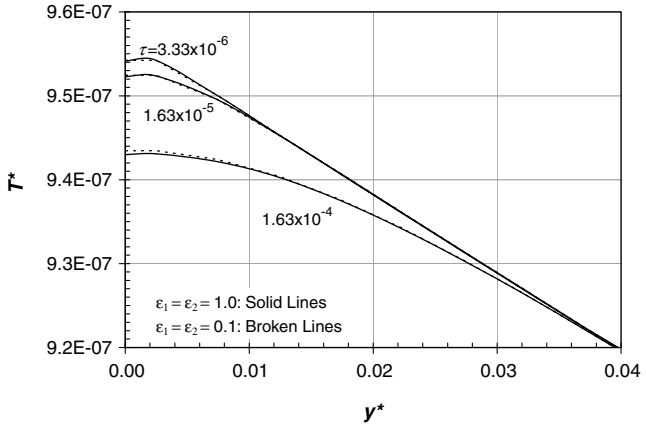

Fig. 10 Centerline temperature profiles in a 1-mm-thick composite ($k_x = 11.1$ W/m · K and $k_y = 0.87$ W/m · K) for two different emissivities using a lower-power laser ($I_o = 2.4$ GW/cm^2).

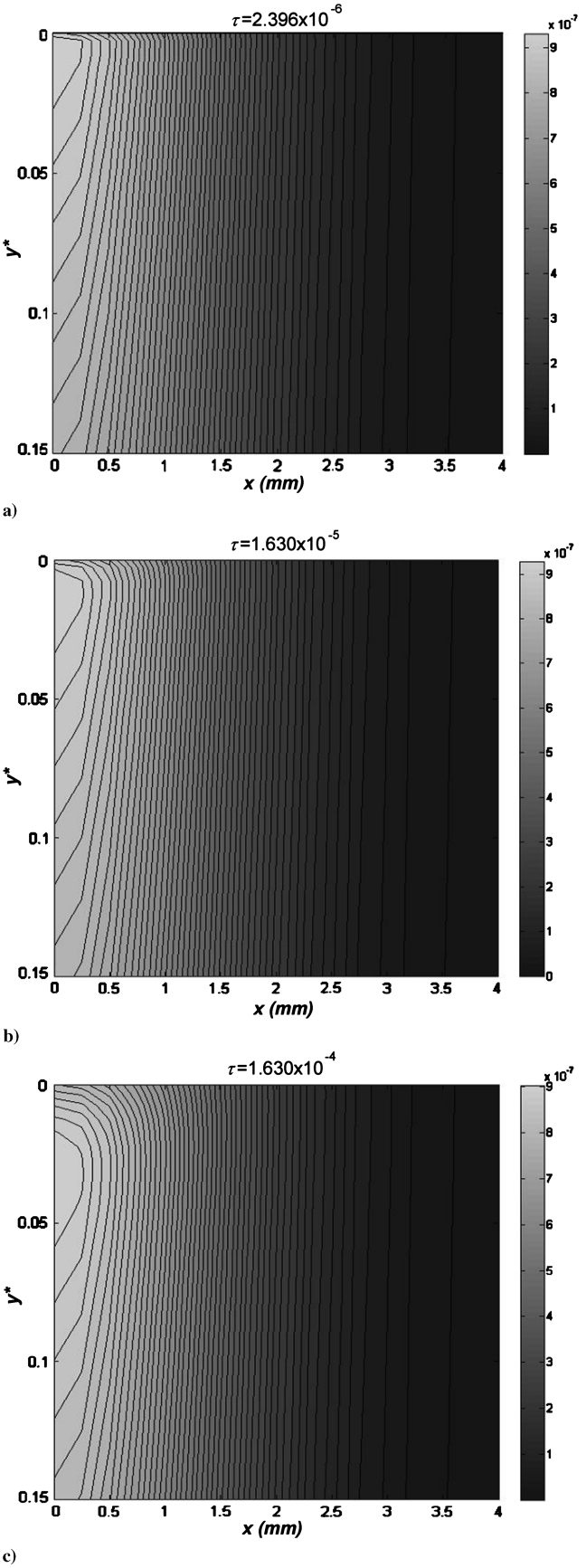

Fig. 11 Two-dimensional temperature profile T^* on 1-mm-thick carbon fiber at a) $\tau = 2.396 \times 10^{-6}$, b) $\tau = 1.630 \times 10^{-5}$, and c) $\tau = 1.630 \times 10^{-4}$.

where $k = 156$ W/m · K, while the broken line corresponds to the composite material properties, with $k_x = 11.1$ W/m · K and $k_y = 0.87$ W/m · K. As in the isotropic case, the peak temperature advances away from the surface as time progresses; this is evident in Fig. 8 for the lower-conductivity material.

2. *Radiation Effects*

Numerical solutions are presented at various time intervals for a material exhibiting orthotropic properties and surface emissivities of $\varepsilon = 1.0$ and 0.1 in Fig. 9. It shows extreme cases of the effect that radiative cooling has on a hot surface that is heated by a high-power laser. If the peak laser power ($I_o = 24$ GW/cm^2) is decreased by one order of magnitude, the effect of the radiative cooling becomes less significant, as shown in Fig. 10. Radiative effects are a strong function of temperature, which is elevated with higher laser power. Radiative cooling effects becomes more evident as the overall temperature and/or surface emissivity increases. As a result, the surface temperatures decrease more rapidly as those two parameters increase.

3. *Temperature Contours*

To help further visualize the spatial temperature distribution T^* within the slab, contour plots, shown in Fig. 11, were created for a 1-mm-thick carbon fiber material at three time steps. Note that the y lengths in these plots are scaled by the penetration depth μ; the total thickness of the material is $y^* = 4.95$ in scaled units. This scaling allows the location of the peak temperature in the plots to be more easily discerned. The lines in the plots represent isotherms, and while the shading indicates the temperature magnitude. Recall that the center of the laser pulse illuminates the slab at $x = 0$ mm and $y^* = 0$. Thus, as expected, the slab is hottest near the origin. The spatial progression of the maximum temperature with time can be seen over the three plots. Initially, the temperature is the hottest near the surface. But as time progresses, the temperature peak shifts inward as the surface cools. By $\tau = 1.63 \times 10^{-4}$, the maximum temperature is located beneath the surface, as shown in Fig. 11c.

Regardless of whether the material has isotropic or orthotropic properties, if the maximum temperature is located within the material, damage due to laser heating may occur without being visible at the material surface. This may have significant impacts on the integrity of the material (e.g., carbon fibers may debond or fray). Furthermore, temperature measurements made at the surface of the material (such as from a thermocouple) may not capture the true maximum temperature excursion, resulting in poor prediction of material integrity. A periodically pulsing laser may, for example, melt the material inside while the surface remains intact.

IV. Conclusions

A thermal model was developed to analyze the temperature distribution within a radiating plate subjected to a spatially and temporally decaying laser. Previous works have considered only the effects of convection on the plate boundaries. Since many high-temperature engineering applications operate in a regime in which radiation heat transfer dominates, the model developed in this study can be a useful tool in determining the thermal response of materials subjected to laser heating.

The temperature profile near the surface is strongly influenced by the thermophysical and optical properties of the material. As expected, the shape of the profile is ultimately a function of the material thermal conductivity and radiation effects. These results show that although the material surface may be cooled while being exposed to an intense laser heating load, a noticeable peak temperature may be achieved beneath the irradiated surface, potentially damaging the material.

Improvements to this model can be made by introducing non-homogeneities in the material, temperature-dependent material properties, and a periodically pulsating laser. Future studies will be made to see how these effects can influence the thermal response of the material.

Appendix: Thermal Model

A thermal math model (TMM) is developed to simulate the one- and two-dimensional partial differential equations that govern the transport of energy. The TMM is a lumped-parameter representation of the heat capacitance and heat transfer paths, which is built with SINDA [10] to predict temperatures as a function of time. SINDA is a finite difference thermal analysis code that consists of a preprocessor and execution library. By following certain rules, the preprocessor reads the SINDA input data file developed by the analyst and constructs a FORTRAN executable. The analyst selects various subroutines from the SINDA library or includes the necessary FORTRAN logic to solve the specific heat transfer problem.

In this model, the SINDA subroutine ATSDUF is selected to obtain the transient solution of the governing nonlinear partial differential equations (1) and (5). ATSDUF is an explicit scheme based on the Dufort–Frankel finite differencing routine with an automatic time-step selection. The basic equation solved by this routine is

$$\left(1 + \frac{(\Delta t)(G_{ij})}{C_i}\right) T_i' = T_i + \sum_{j=1}^{n} \frac{(\Delta t)(G_{ij})}{C_i} T_j - \sum_{j=1}^{n} \frac{\Delta t}{C_i} G_{ij} T_i'' + \frac{\Delta t}{C_i} Q_i \tag{A1}$$

where n, i, and j denote the total number of nodes, current node, and adjacent node, respectively; T, T', and T'' denote the present, unknown (future), and past temperatures, respectively; C_i is the node capacitance; Q_i is the heat source; and G_{ij} represents either the linear or radiation conductance. Caution should be taken when implementing automatic time-step routines, because the time scales involved in this problem are very small (on the order of nanoseconds). Proper time steps need to be taken to ensure that the solution converges correctly while the runtimes are kept to a tolerable level. The time steps taken for this analysis were approximately 10^{-10} s, with runtimes on the order of a few minutes for each case to complete.

In the case of thermal radiation, the following quasi-linear approximation is used to calculate the radiation conductance:

$$G_{ij} = \sigma A_i F_{ij} (T_i^2 + T_j^2)(T_i + T_j) \tag{A2}$$

Since the slab surface is assumed to have a full view to the environment, the view factor F_{ij} is equal to unity. One outstanding feature of ATSDUF is that it automatically selects the time step based on the specification of three subroutine parameters: ERRMIN (0.003°C), ERRMAX (0.006°C), and TSD. The value of TSD, which is the maximum second derivative term for a given time step, is calculated by using

$$\text{TSD} = \frac{\partial^2 T}{\partial t^2} \frac{\Delta t^2}{2} \tag{A3}$$

The temperature iterations are repeated and the old ones are discarded. This process will continue until TSD < ERRMAX.

References

[1] Blackwell, B. F., "Temperature Profile in Semi-infinite Body with Exponential Source and Convective Boundary Condition," *Journal of Heat Transfer*, Vol. 112, Aug. 1990, pp. 567–571. doi:10.1115/1.2910424

[2] Ready, J. F., *Industrial Applications of Lasers*, Academic Press, New York, 1978.

[3] Dabby, F. W., and Paek, U., "High-Intensity Induced Laser Vaporization and Explosion of Solid Material," *IEEE Journal of Quantum Electronics*, Vol. *QE-8*, No. 2, 1972, pp. 106–111. doi:10.1109/JQE.1972.1076937

[4] Chaudhry, M. A., and Zubair, S. M., "Conduction of Heat in a Semi-Infinite Solid with an Exponential-Type Initial Temperature Profile: Temperature and Heat Flux Solutions Due to an Instantaneous Laser Source," *Wärme- und Stoffübertragung*, Vol. 30, No. 1, 1994, pp. 41–46. doi:10.1007/BF02347002

[5] Zubair, S. M., and Chaudhry, M. A., "Heat Conduction in a Semi-Infinite Solid When Subjected to Spatially Decaying Instantaneous Laser Source," *Wärme- und Stoffübertragung*, Vol. 28, No. 7, 1993, pp. 425–431.
doi:10.1007/BF01577884

[6] Zubair, S. M., and Chaudhry, M. A., "Heat Conduction in a Semi-Infinite Solid Due to Time-Dependent Laser Source," *International Journal of Heat and Mass Transfer*, Vol. 39, No. 14, 1996, pp. 3067–3074.
doi:10.1016/0017-9310(95)00388-6

[7] Yilbas, B. S., "A Closed-form Solution for Temperature Rise Inside Solid Substrate Due to Time Exponentially Varying Pulse," *International Journal of Heat and Mass Transfer*, Vol. 45, No. 9, 2002, pp. 1993–2000.
doi:10.1016/S0017-9310(01)00281-2

[8] Cheung, T. K., Blake, B. A., and Lam, T. T., "Heating of Finite Slabs Subjected to Laser Pulse Irradiation and Convective Cooling," *Journal of Thermophysics and Heat Transfer*, Vol. 21, No. 2, Apr.–June 2007, pp. 323–329.
doi:10.2514/1.23100

[9] Peterson, L. A., Cheung, T. K., Lam, T. T., and Blake, B. A., "Heat Conduction in Two-Dimensional Slabs Subjected to Spatially Decaying Laser Pulses," *Journal of Thermophysics and Heat Transfer*, Vol. 23, No. 1, Jan.–Apr. 2009, pp. 18–27.
doi:10.2514/1.29986

[10] SINDA/G, Software Package, Ver. 2.5, Network Analysis, Inc., Chandler, AZ, 2006.

[11] Chambré, P. L., "Nonlinear Heat Transfer Problem," *Journal of Applied Physics*, Vol. 30, No. 11, Nov. 1959, pp. 1683–1688.
doi:10.1063/1.1735036

[12] Siegel, R., and Howell, J. R., *Thermal Radiation Heat Transfer*, 4th ed., Taylor and Francis, Philadelphia, 2002.

[13] Özisik, M. N., *Heat Conduction*, 2nd ed., Wiley, New York, 1993, Chaps. 2 and 13.

[14] *ASM Handbook*, Vol. 2, ASM International, Materials Park, Ohio, 1990.

[15] Palik, E. D., *Handbook of Optical Constants of Solids*, Academic Press, New York, 1985.

[16] Incropera, F. P., and DeWitt, D. P., *Fundamentals of Heat and Mass Transfer*, 5th ed., Wiley, New York, 2002.